International Journal of Electrical, Electronic and Communication Sciences
ISSN: 2517-9438
Vol:13, No:8, 2019

Modelling and Simulating CO_2 Electro-Reduction to Formic Acid Using Microfluidic Electrolytic Cells: The Influence of Bi-Sn Catalyst and 1-Ethyl-3-Methyl Imidazolium Tetra-Fluoroborate Electrolyte on Cell Performance

Akan C. Offong, E. J. Anthony, Vasilije Manovic

***Abstract*—**A modified steady-state numerical model is developed for the electrochemical reduction of CO_2 to formic acid. The numerical model achieves a CD (current density) (~60 mA/cm^2), FE-faradaic efficiency (~98%) and conversion (~80%) for CO_2 electro-reduction to formic acid in a microfluidic cell. The model integrates charge and species transport, mass conservation, and momentum with electrochemistry. Specifically, the influences of Bi-Sn based nanoparticle catalyst (on the cathode surface) at different mole fractions and 1-ethyl-3-methyl imidazolium tetra-fluoroborate ([EMIM][BF_4]) electrolyte, on CD, FE and CO_2 conversion to formic acid is studied. The reaction is carried out at a constant concentration of electrolyte (85% v/v., [EMIM][BF_4]). Based on the mass transfer characteristics analysis (concentration contours), mole ratio 0.5:0.5 Bi-Sn catalyst displays the highest CO_2 mole consumption in the cathode gas channel. After validating with experimental data (polarisation curves) from literature, extensive simulations reveal performance measure: CD, FE and CO_2 conversion. Increasing the negative cathode potential increases the current densities for both formic acid and H_2 formations. However, H_2 formations are minimal as a result of insufficient hydrogen ions in the ionic liquid electrolyte. Moreover, the limited hydrogen ions have a negative effect on formic acid CD. As CO_2 flow rate increases, CD, FE and CO_2 conversion increases.

***Keywords*—**Carbon dioxide, electro-chemical reduction, microfluidics, ionic liquids, modelling.

I. Introduction

THERE is a clear correlation between rising CO_2 concentration in the atmosphere and currently observed changes in the global climate. In 2018, anthropogenic annual CO_2 emissions were estimated to be about 36.8 billion tons with concentrations approaching 408.71 ppm [1]. However, increased usage of CO_2 as a building block for carbon-based compounds and materials can provide a stepping stone in moderating worldwide CO_2 emissions. Typically, CO_2 conversion is achievable by chemical, photochemical, and electrochemical reduction methods. In recent years, CO_2 conversion using electrochemical approaches has gained considerable attention for several advantages. Primarily, CO_2 electrochemical reactions are easily controlled by electrode potentials, reaction pressure, pH and temperature. Secondly, its supporting electrolyte is fully recyclable; its overall chemical consumption is reducible to water or wastewater. Thirdly, electricity used to drive the reaction is obtainable without generating CO_2 e.g. from solar, wind, hydroelectric, geothermal, tidal, and thermo-electric sources [2], [3]. Finally, electrochemical reaction systems are compact, modular, on-demand, and easy for scale-up applications. Increasing efforts have been devoted to CO_2 electro-reduction using microfluidic technology (MEC─ Microfluidic Electrolytic Cell). This stems from the primary reasons that MECs eliminate sweep away effect of the flowing electrolyte, reduce carbonate formation, and electrode dry-out/flooding [2]-[4]. Formic acid, the desired product in this study recovered by liquid-liquid extraction from the MEC electrolyte is the most significant organic compound to be formed from ECRC─ Electrochemical Reduction of Carbon. Besides, formic acid represents a suitable storage media for intermittent sources of energy as prospective electrolytes in battery cells [2], [3]. Taking a look at CO_2 electro-reduction using MECs, current developments in literature are discussed, covering both experiments and mathematical models. In addition, MFC (Microfluidic Fuel Cell) models are discussed, due to the fact that, an MFC operated in a reverse is an MEC.

In 2005, the first computational model for MFCs was developed. It was considered a T-shaped formic acid MFC with side-by-side streaming but suggested methods to improve the electrodes were made [5]. In 2006, an extended theoretical model was developed which included a Butler-Volmer model for the electro-kinetics in a Y-shaped formic acid/dissolved oxygen based cell [6]. A similar model for the planar was presented in 2006, moreover, completed by a 2D theoretical model of cathode kinetics in a co-laminar flow [7]. In 2007, a Butler Volmer model was developed for the MFC employing

Vasilije Manovic is a Professor of Carbon Systems Engineering, currently with the Centre for Combustion and CCS, Cranfield University, Cranfield, MK43 0AL, UK (corresponding author, phone:+44(0)1234754689 e-mail: v.manovic@cranfield.ac.uk).

A. Offong is doctoral researcher currently with the Carbon Capture and Storage Department, Cranfield University, Cranfield, MK43 0AL, UK (e-mail: a.offong@ cranfield.ac.uk).

E.J. Anthony is a Professor of Energy Process Systems, currently with the Centre for Climate and Environmental Protection, Cranfield University, Cranfield, MK43 0AL, UK (e-mail: b.j.anthony@cranfield.ac.uk).

hydrogen peroxide as fuel examining the effects of specie transport and geometrical design [8]. A crude cathode model for electro-reducing CO_2 to potassium formate in a continuous "trickle-bed" reactor with Sn catalyst was also presented followed by model for CO_2 electro-reduction in a solid oxide electrolysis cell using Ni catalyst [9], [10]. In 2008, a 3D steady-state and isothermal model with a trident-shaped microchannel geometry was developed to determine the optimum geometry in enhancing reactant distribution and fuel utilization [11]. In 2010, a 3D model was developed to compare flow and heat transfer characteristics in symmetric/ asymmetric tree-like branching networks with symmetric/ asymmetric leaf-like branching network in-cooperated in heat sinks. This led to the conclusion that asymmetry minimally influenced the tree-like branching network at low branching numbers [12]. In the same year, a very comprehensive numerical study was made using different 3D numerical models developed for different MFCs, in order to determine the effect of different modifications that have been implemented since its introduction. The modifications included channel geometry aspect ratio, electrolyte configuration, a flow between anolyte and catholyte in the channel and a multiple placed inlets [13]. An air-breathing MFC was also presented which assumed a constant oxygen concentration resulting in the poor consideration of the naturally and forced convective mass transfer resistance in the gas phase [14]. Finally, a detailed model was proposed for electro-reducing CO_2 to CO in a cell similar to a proton-exchange-membrane fuel cell including an additional aqueous $KHCO_3$ buffer layer [15]. In 2011, a similar study which entailed a numerical model to predict transport and reaction patterns, and electrochemical performance under different pH for an air-breading reversible MFC was carried out [16]. In the same year, the same research group presented a more detailed numerical model based on a forced-air-convection MFC [17]. In addition, a computational model for a microfluidic cell consisting of flow-through porous electrodes was developed. The model which included fluid-flow, mass transport and electrochemical kinetics was coupled and solved with first principles in COMSOL Multiphysics [18]. In 2013, the same research group presented a comprehensive theoretical model studying air-breathing MFCs using a semi-empirical Graetz-Domkohler analysis [19]. This research was accompanied by a numerical analysis of the MFC geometry and operation using finite-element simulations [20]. However, in the same year, a model was developed for CO_2 electro-reduction to formic acid in an MEC using Sn catalyst, the computational approach for simulating the electrode-electrolyte interface was unclear with potential distribution and definition of over-potentials oversimplified [8]. In 2014, a 3D computational model for air-breathing MFCs with flow-over and flow-through anodes was presented. This model studied the phenomena of fluid flow, species transport and electrochemical reactions [21]. Followed by a hierarchical multiscale model for vanadium MFCs, this model incorporated porous electrodes, where diffusion coefficient was used as bridge between microscale, mesoscale and macroscale using three-level-theories setup [22]. In 2015, an agglomerate model for performing a comprehensive electrochemical simulation of a cathode layer was presented. The model could predict cell performance at high CD which was not the case using homogeneous model [23]. In the same year, follow-up study was presented, which aimed at developing a 2D mathematical framework at steady state/isothermal for modelling electro-chemical conversion of CO_2 to CO using Ag catalyst in an MEC [24]. In 2017, a comparative numerical study between co-flow and counter flow cell was made, which revealed that short and wide electrodes were more appropriate for counter flow MFCs rather than conventional long and narrow ones. Nonetheless, counter flow MFC exhibits great advantages on low flow rate tolerance, contributing to an improved energy density and fuel utilization. Summary of electrochemical performance in CO_2 conversion to formic acid till date shows the highest recorded formic acid CD of 150 mA/cm^2, FE of 98%, and CO_2 conversion of 50% [25]. However, from literature, there is currently no published research showing all three simultaneously optimised model performance measures; FE ($\geq$ 80 %), CD ($\geq$ 100 mA /cm^2) and CO_2 conversion ($\geq$ 80 %) in the electro-reduction of CO_2 to formic acid [2], [3], [5], [14], [16], [25]-[27]. Moreover, modelling and simulating the electrochemical conversion of CO_2 to CO, and HCOOH in microfluidic reactors seemed complex and challenging. This complexity was attributed to the insufficient understanding of underlying fundamental integrations in the cell and their influence on cell performance. Understanding fundamental underlying integrations using mathematical models is of great importance for development of MECs since experimental work does not reveal this.

In this study, an approach using desired composition ratio Bi-Sn nanoparticle catalyst and [EMIM][BF_4] ionic liquid electrolyte in a modified microfluidic electrolytic model is carried out to find out strategies of maximizing formic acid FE, and CD, and CO_2 conversion simultaneously. Bi and Sn nanoparticle catalyst from literature has been proven to be selective in formic acid production from CO_2 electro-reduction with high HER (Hydrogen Evolution Reaction) over-potentials [28]. In addition, [EMIM][BF_4] ionic liquid electrolyte with favourable characteristics including high ionic conductivity, thermal stability and low water content, contributes to high formic acid CD suppressing hydrogen evolution- a side reaction. This brings us to a better understanding of the fundamental integrations/reactions electrochemical characteristics coupled with MEC processes. The model covers transport of species and charges, momentum, mass conservation and electrochemical reaction kinetics with competing hydrogen reaction emphasizing on the cathode side. Model-based parametric analysis is also carried out to find optimize overall cell performance.

II. Mathematical Formulation

We consider the microfluidic electrochemical cell of Fig. 1, which is equipped with parallel, rectangular, multi-layered channels, and operates in a co-flow mode. A stream of CO_2 enters the cathode gas channel, while the anode is open to the

atmosphere. An ionic liquid electrolyte [EMIM][BF_4] flows between two gas diffusion electrodes (GDEs). The cathode is coated with a Bi-Sn nanoparticle catalyst, while the anode is coated with Pt blank at the electrode-electrolyte interface. A graphite current-collector backs each GDE at the other side. The model is calibrated and validated using experimental data from literature, and the sensitivity of several designs and operating variables is analysed via simulations. COMSOL Multiphysics software is implemented in modelling using base-case parameter values and solved using finite element method.

A. Electrode Reactions

To reduce CO_2 to formic acid in a microfluidic cell, we supply current to the microfluidic cell, and the following electrochemical reactions occur [24]:

At the anode:

$$2OH^- \rightarrow 0.5O_2 + H_2O + 2e^- + 0.82\ V \text{ vs. SHE—Standard Hydrogen Electrode} \quad (1)$$

At the cathode:

$$CO_{2\,(aq)} + H_2O + 2e^- \rightarrow HCOOH \quad -0.613\ V \text{ vs. SHE} \quad (2)$$

$$2H_2O + 2e^- \rightarrow H_2 + 2OH^- \quad -0.41\ V \text{ vs. SHE} \quad (3)$$

Note, water reduces to H_2 gas via (3), but the H_2 produced is negligible since an ionic liquid is the desired electrolyte used.

Numerical simulation is based on the following assumptions and simplifications [15], [21], [24];

1. The system is isothermal and at a steady-state. Therefore is a reasonable assumption for an electrochemical cell with a flowing electrolyte.
2. Electrolyte used is an incompressible Newtonian fluid with laminar flow.
3. Gas used is weakly compressible with laminar flow.
4. Side walls of the cell are impermeable, with zero slip.
5. Concentrations do not vary along the cell cross-section.
6. We impose no slip and zero species flux at the left and right cell walls.
7. The overall internal environment of the cell is purged with nitrogen before start, therefore assumed neutral.

Considering transport in gas channels, porous GDEs, and electrolyte; material balance in the gas phase (cathode: CO_2, and H_2; anode: O_2) and electrolyte liquid phase (H^+, OH^-, $HCOO^-$, $[EMIM]^+$, $[BF_4]^-$), the electric and ionic charge balance; and charge transfer kinetics gives us the following conservation equations [24]:

$$\nabla \cdot (\rho \mathbf{u}) = 0 \quad (4)$$

$$\nabla\rho = \begin{cases} -\rho\mathbf{u}\cdot\nabla\mathbf{u} + \nabla\cdot\left(\mu(\nabla\mathbf{u} + (\nabla\mathbf{u})^{\tau}) - \frac{2}{3}\mu(\nabla\cdot\mathbf{u})\mathbf{I}\right) & \text{(Gas channel)} \\ \frac{\rho}{\varepsilon}\left((\mathbf{u}\cdot\nabla)\frac{\mathbf{u}}{\varepsilon}\right) + \nabla\cdot\left[\frac{1}{\varepsilon}\left(\mu(\nabla\mathbf{u} + (\nabla\mathbf{u})^{\tau}) - \frac{2}{3}\mu(\nabla\cdot\mathbf{u})\mathbf{I}\right)\right] - \left(\frac{\mu}{\kappa}\right)\mathbf{u} & \text{(GDE)} \\ -\rho\mathbf{u}\cdot\nabla\mathbf{u} + \mu\nabla^2\mathbf{u} + \rho\mathbf{g} & \text{(electrolyte)} \end{cases} \quad (5)$$

$$\nabla \cdot \mathbf{ni} = 0 \quad (6)$$

$$\nabla \cdot \mathbf{i} = 0 \quad (7)$$

where ρ, $\mathbf{u}$, τ, $\mathbf{g}$, D_i, ε, n_i, μ and $\mathbf{i}$ respectively denote the density of fluid (kg/m^3), velocity (m/s), stress tensor (Pa), acceleration due to gravity (9.8 m/s^2), diffusivity of species i (m^2/s), porosity, electron transfer number, dynamic gas viscosity and CD of species.

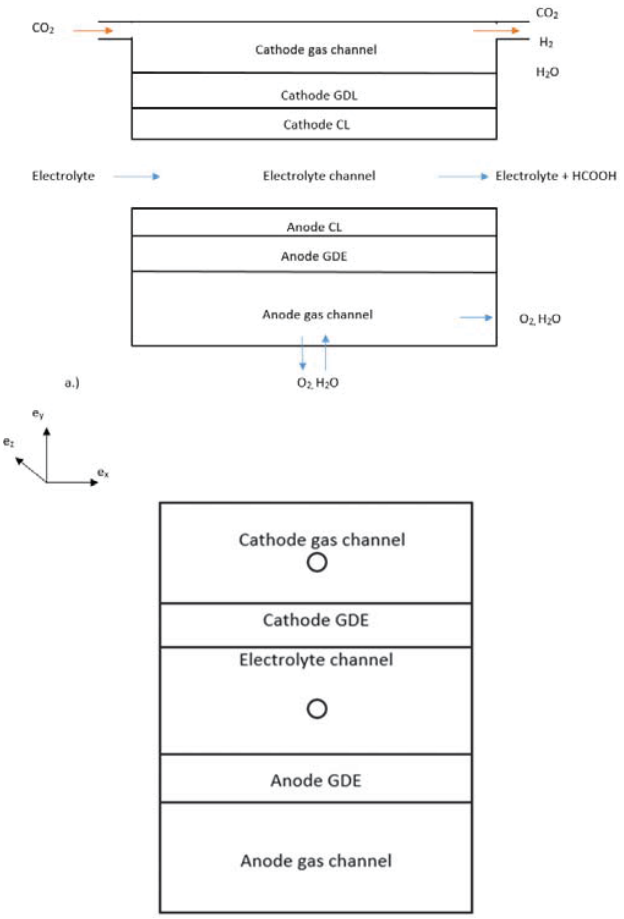

(b)

Fig. 1 Schematics of (a) the front and (b) the side view of a microfluidic electrochemical cell

Accounting for diffusion and convection in the cathode; however, only diffusion in the anode is considered due to an open boundary. In the electrolyte, we consider convection, diffusion, and the migration of charged species. Then, molar fluxes of the various species are as follows [24]:

$$\boldsymbol{n}_i = \begin{cases} -\rho D_i \nabla\omega_i + (\rho\mathbf{u}\omega_i) & \text{(Cathode)} \\ -\rho D_i \nabla\omega_i & \text{(Anode)} \\ -D_i\nabla C_i - Z_i u_{m,i} C_i \nabla\phi_l + C_i\mathbf{u} & \text{(Electrolyte)} \end{cases} \quad (8)$$

(Cathode: $i = CO_2, H_2$)
(Anode: $i = O_2$)
(Electrolyte: $i = H^+, HCOO^-, OH^-, [EMIM]^+, [BF_4]^-$)
where ω_i, the mass fraction of species i, D_i, the multicomponent diffusion coefficient, ϕ_l, the electric potential of the liquid

electrolyte, C_i, the local electrolyte concentration of species *i*.

We define the current densities at the electrodes and in the electrolyte [24]:

$$i = \begin{cases} -\sigma_s \nabla \emptyset_s & \text{(GDEs)} \\ F \sum_i z_i \left(-D_i \nabla C_i - z_i u_{m,i} C_i \nabla \emptyset_l\right) & \text{(Electrolyte)} \end{cases} \quad (9)$$

(Electrolyte: $i = H^+$, $HCOO^-$, OH^-, $[EMIM]^+$, $[BF_4]^-$)

where ϕ_s and ϕ_l are the local electrode and electrolyte potential, σ, electric conductivity (S/m), C_i, the local electrolyte concentration, F, the Faraday's constant, z_i, the electron transfer number of the rate determining step, and u_m, average normal inflow velocity.

The electro-kinetics associated with (1)-(3) depends on CO_2 concentration, electrolyte temperature, conductivity [24]:

$$i_{HCOOH} = 2F k_{HCOOH} C_{CO2} \exp\left(-\frac{2\alpha_{HCOOH} F}{RT} \eta_{HCOOH}\right) \quad (10)$$

$$i_{H2} = i_{H2}^{ref} \exp\left(-\frac{2\alpha_{H_2} F}{RT} \eta_{H2}\right) \quad (11)$$

$$i_{O2} = i_{O2}^{ref} \exp\left(-\frac{2\alpha_{O_2} F}{RT} \eta_{O2}\right) \quad (12)$$

where $i_{HCOOH,ref}$ is the HCOOH exchange CD, C_{CO2}, the local CO_2 concentration, $C_{CO2,ref}$, the reference CO_2 concentration, α_{HCOOH}, the charge transfer coefficient, F, the Faraday's constant, R, the universal gas constant, α, the charge transfer coefficient, k, the permeability of the electrode, T, the system temperature, and η_{HCOOH}, the over-potential of HCOOH formation reaction at the cathode.

The over-potentials of various species at the triple-phase-boundaries are given by the difference between the potential driving difference and the reversible potential of the half-cell [24].

$$\eta_i = \emptyset_s - \emptyset_l - E_i \quad (13)$$

(i = HCOOH, H_2, O_2)

where E_{HCOOH} is the reversible potential of the half reaction for HCOOH formation, ϕ_s and ϕ_l are local electric and electrolyte potential, η_i, the over-potential of species *i*.

For boundary conditions, constant compositions and flow rates at the inlets is ensured; constant reference pressure with no diffusive species fluxes at outlets; zero slip and flux at the cathode gas channel walls; charge insulation and zero slip at the GDEs vertical walls; constant potentials at electrode-gas channel interface; molar fluxes and current densities at the electrode/electrolyte interfaces.

The numerical model above was implemented in COMSOL Multiphysics, with base case parameter values shown in Table I, and solved using the finite element method.

B. Model Input Parameters

Fundamental input parameters for model simulations are obtained from literature and summarised in Table I. Novel materials include Bi-Sn nanoparticle catalyst and $[EMIM][BF_4]$ ionic liquid electrolyte.

TABLE I
KEY INPUT PARAMETERS OF THE MODEL

Parameter	Value	Unit	Ref.
Temperature	298	K	[24]
Exit Pressure	101.3	kPa	[24]
Electrolyte flow rate	0.7	ml/min	[24]
Charge transfer coefficient of HCOOH formation half-cell	-0.05	-	[21]
Charge transfer coefficient of H_2 formation half-cell	-0.5	-	[21]
Charge transfer coefficient of O_2 formation half-cell	0.16	-	[21]
Exchange CD at cathode HCOOH formation	0.1	A/m^2	[21]
Channel Length	0.015	m	[21]
Channel Width	0.025	m	[24]
Height of cathode gas channel	5.08E-4	m	[24]
Height of the cathode GDL	3E-4	m	[24]
Height of the electrolyte channel	0.0015	m	[24]
Electrolyte ionic conductivity	5.5E-6	S/m	[29,30]
Diffusion coefficient of CO_2	9.8E-4	m^2/s	[26,31]
Porosity of cathode GDL	0.4	-	[24]
Permeability of the cathode GDL	10^{-12}	H/m	[3]

C. Materials Used in Model

- Electrodes; anode (platinum) and cathode (Bi-Sn alloy)
- Bi-Sn nanoparticle catalyst
- 85 % v/v. $[EMIM][BF_4]$ electrolyte
- CO_2 gas

III. RESULTS AND DISCUSSION

A. Model Validation

Model validation is carried out by comparing anode and cathode performances individually. Model simulations are compared with experimental results from [2]. Computed results agree well with both experimental and theoretical results in literature.

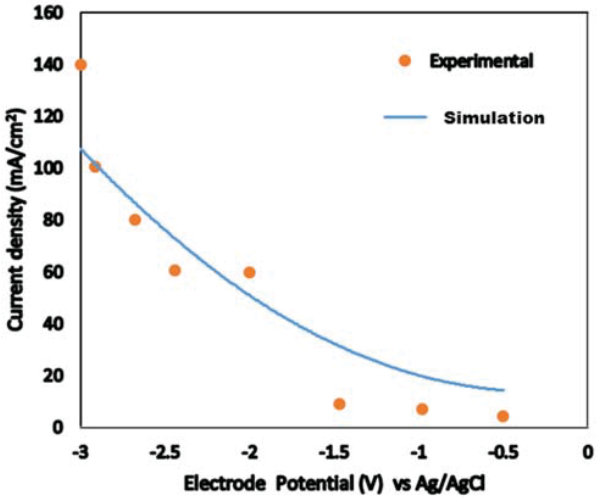

(a)

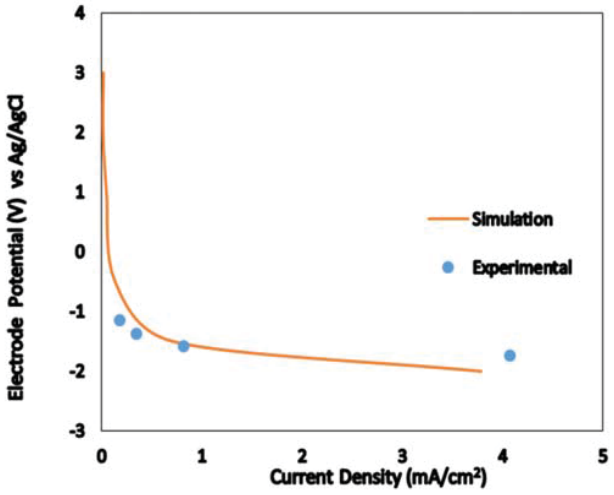

(b)

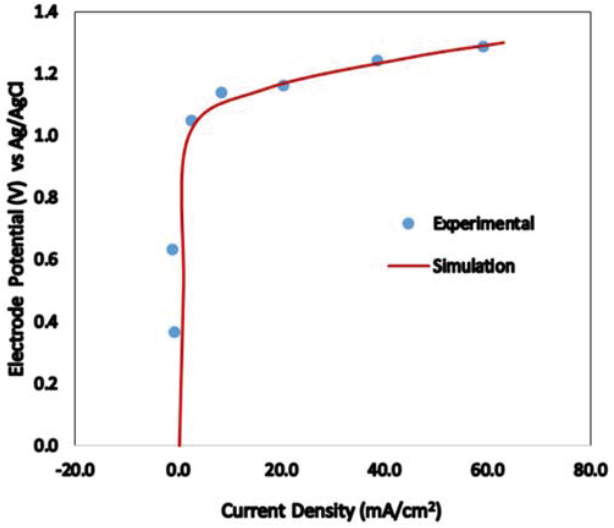

(c)

Fig. 2 Comparison of (a) Cathodic HCOOH CD (b) Cathodic H_2 CD (c) Anodic O_2 CD from numerical results and experimental data

B. Mass Transfer Characteristics

In the MEC, the cathode, where CO_2 is reduced to formic acid is a critical component in determining the cell performance and chemical efficiencies, and is the primary focus of this work. The cathode-CL is comprised of a bimetallic nanoparticle catalyst at varying mass ratios. The electrolyte used is an ionic liquid ([EMIM][BF_4]) with concentration of 85 % v/v.

1) Mass Transfer Characteristics with Bi-Sn Nanoparticle Catalyst at Varying Weight Ratios

Concentrations of CO_2 and H_2 (negligible) distributions inside the gas channel and the GDE are calculated, with contours shown in Figs. 3 (a)-(g).

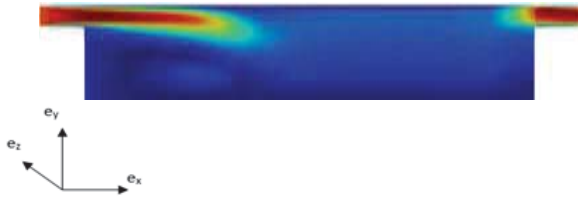

Fig. 3 Concentration contour of CO_2 in gas channel (mol/m^3): mole ratio 0.5:0.5 Bi-Sn particle catalyst;

C. Electrochemical Characteristics

The different electric conductivities of Bi-Sn catalyst at different mole ratios have an impact on the concentration contours of CO_2 in the gas channel. By order of the highest electric conductivity, the catalysts mole ratios are as thus; 0.7:0.3 > 0.2:0.8 > 0.3:0.7 > 0.05:0.95 > 0.4:0.6 > 0.025:0.975 > 0.5:0.5. However, it is noted that 0.5:0.5 Bi-Sn catalyst mole ratio on the cathode electrode displays optimum CO_2 consumption in reaction. Therefore, this research concentrated on mole ratio 0.5:0.5 Bi-Sn catalyst. Fig. 4, presents a simulated CD -potential. Increasing the negative cathode potential increases the current densities for both HCOOH and H_2 formations.

Here, HER is a competing reaction with little or almost no impact on the main cathode reaction at pH 7 with current densities of 0 to 2.5 mA/cm^2. However, from Figure 4, it is clear that there is a correlation between an increased negative electrode potential and increased HER. This in turn, leads to a high FE for HCOOH formation. Thermodynamically, HER occurs immediately the cathode potential is lower than -1.02 V vs. SHE [3]. However, our results reveal that HER occurs as the potential drops below 1 V. This is attributed to the high electric conductivity of the electrolyte although HER kinetically should take place after -1.02 V due to small exchange CD. The HER partial CD in Figure 4 is about two orders of magnitude lower than HCOOH partial CD. Further increase in the applied over-potential does not substantially increase HER; this is attributed to the lack of sufficient H^+ in the ionic liquid electrolyte and at the selective cathode catalyst interface. On the other hand, when a higher negative over-potential is applied for HCOOH formation, HCOOH CD increases as a result of optimum catalyst composition applied, high electrolyte CO_2 solubility [32,33], and electrolyte ionic conductivity for CO_2 electro-reduction reaction. Moreover, the cationic species of the electrolyte contributes to increased FE and CD of the reaction process. This is attributed to its high formic acid selectivity as a result of high affinity for CO_2 molecules [27].

D. Effect of HER Kinetics

HER can greatly reduce the MEC performance via two mechanisms, i.e. cathode reaction competition and dilution of CO_2. Efforts have been devoted to suppressing the HER by coating a more selective cathode catalyst and using an ionic liquid electrolyte. These efforts fundamentally aim to reduce the exchange CD of HER. The effect of HER exchange CD on current efficiency is studied. In the literature, experimental data showed that the superficial HER exchange CD on porous GDE

structures lies typically in a range of 0.01 to 1 mA/cm^2 [2]. It is found in Fig. 5, that the impact of HER on the FE of MEC is relatively small with the FE averaging 94.34%. A high efficiency would imply that eliminating HER by employing appropriate electrolyte and selective catalysts is key.

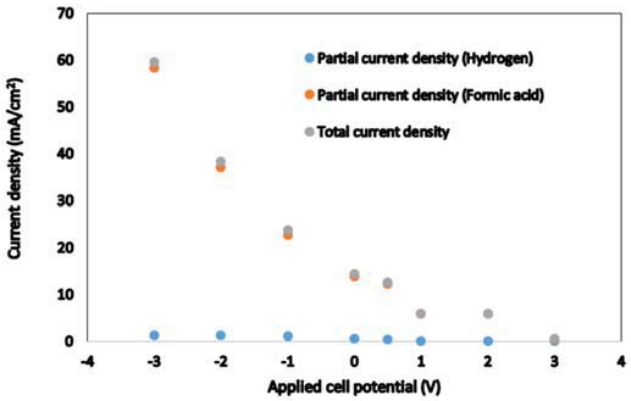

Fig. 4 Cathode total CD, HCOOH partial CD and HER partial CD versus electrode potential at 85% v/v. [EMIM][BF$_4$] electrolyte

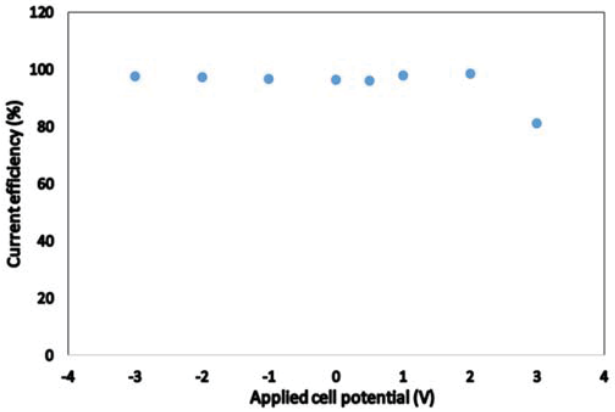

Fig. 5 Cathode FE for formic acid versus electrode potential using [EMIM][BF$_4$] ionic liquid electrolyte

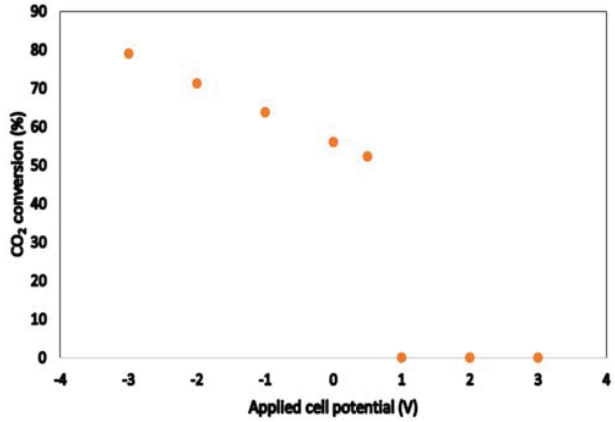

Fig. 6 CO_2 conversion versus applied potential using [EMIM][BF$_4$]

E. Effect of Channel Length

Figs. 8 (a) and (b), show the effect of channel length on CO_2 consumption/reaction in the cathode gas channel. Fig. 8 (a), shows an initial CO_2 concentration of 0.055 mol/m^3 at the inlet, before peaking to 0.07 mol/m^3 at 0.002 m x-direction before gradually decreasing along the entire gas channel. In Fig. 8 (b), CO_2 concentration spikes from 0.07 mol/m^3 to 0.085 mol/m^3 at about 0.0018 m x-axis direction from inlet, before decreasing exponentially along the entire gas channel. The high CO_2 consumption is attributed to increased residence time in the gas channel and a longer channel improves CO_2 conversion [24]. However, while a longer gas channel increases CO_2 conversion it does so at the expense of the CD and FE.

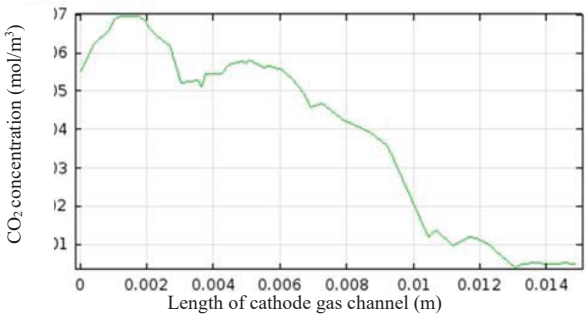

(a)

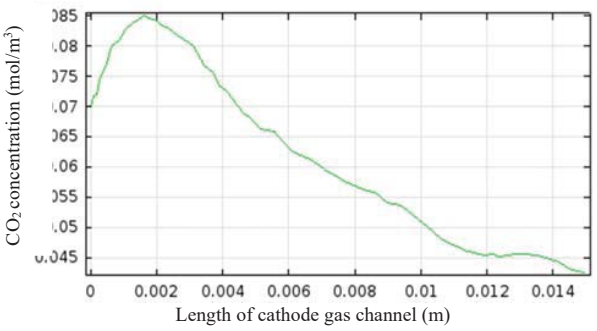

(b)

Fig. 8 CO_2 concentration contour along the x-axis of cathode gas channel at 0.0028 S/m cathode catalyst─(a) Channel length of 0.015 m. (b) Channel length of 0.35 m

IV. Conclusions

A first-principles electrochemical model for CO_2 reduction to formic acid in a microfluidic cell was presented and validated. It accounts for all significant physics and electrochemistry such as momentum and mass conservation, transport of species and charges at the cathode side of the MEC. It is found that high FE is attributed to high diffusion of CO_2 in the GDE porous media and elimination of HER. After parametric analysis were performed using increased channel length, increased gas flow velocity, and increased in feed CO_2 concentration, it was evident that there was a trade-off between three performance measures; FE, CD and CO_2 conversion. These performance measures indicted CO_2 transport and surface catalyst contact

are key in CO_2 electro-reduction rather than just catalyst selectivity. Improved MEC design includes a cell geometry included in Table 1, 0.5:0.5 Bi-Sn catalyst mole ratio, 85 % v/v. [EMIM][BF_4] ionic liquid electrolyte, cathode gas channel length of 0.35 m, and CO_2 gas flow velocity of 0.1 m/s and a feed CO_2 concentration of 0.25 mol/m^3. However, the design didn't provide satisfactory formic acid CD (~60 mA/cm^2). The former is attributed to hydrogen evolution, while the latter is attributed to insufficient hydrogen ions available in the electrolyte to produce formic acid. Moreover, FE (~98%) and CO_2 conversion (~80, ~90 %) at −3 V and 2 V vs. SHE was satisfactory. This provides basis for further optimization with the aim of increasing formic acid FE.

Appendix

List of Abbreviations

CD Current Density
CL Catalyst Layer
ECRC Electro-Chemical Reduction of Carbon
FE Faradaic Efficiency
GDE Gas Diffusion Electrode
GDL Gas Diffusion Layer
MEC Microfluidic Electrolytic Cell
MFC Microfluidic Fuel Cell
SEM Scanning Electron Microscope
SHE Standard Hydrogen Electrode

Nomenclature

C_i concentration of species i, mol/m
D_{ij} multicomponent diffusion coefficients, m^2/s
E_i reversible potential of the half-cell corresponding to formation of species i, V
F Faradaic constant, 96485 C/mol
g acceleration due to gravity, m/s^2
i CD, A/m^2
i_i transfer CD corresponding to the formation of species i, A/m^2
$i_{i,ref}$ exchange CD corresponding to the formationof species i, A/m^2
M_i molecular mass of species i, kg/mol
$\mathbf{n}_i$ mass flux of species i, kg/(m^2·s)
p pressure of gas, Pa
Q mass source term, kg/(m^3·s)
R universal gas constant, 8.314 J/mol·K
T temperature, K
u velocity, m/s
u velocity in the x direction / stream wise direction, m/s
$U_{g,in}$ average normal inflow velocity, m/s
v velocity along the y direction / normal direction, m/s
v_i diffusion volume of molecule i, used in the correlation by Fuller, Schettler, and Giddings
x_i molar fraction of species i
α fitting parameter for through-plane diffusion in the Tomadakis-Sotirchos model
α_i charge transfer coefficient of the half-cell corresponding to the formation of species i
ε porosity of the gas diffusion layer or catalyst layer
η_i over-potential of the formation reaction species i , V
κ permeability of the gas diffusion layer or catalyst layer, m
λ eigenvalues
μ dynamic viscosity, kg/m·s
ρ density of gas, kg/m^3
σ electric/ionic conductivity, S/m
ϕ electric potential
ω_i mass fraction of species i
Ω modified Damkohler number, modified the dimensionless constant Damkohler by a length scale.

Acknowledgment

This work is supported by the Carbon Capture & Storage Department, School of Water, Energy and Environment.

References

[1] Laboratory ESR., Division GM. Trends in Atmospheric Carbon Dioxide. Global Greenhouse Gas Reference Network. 2018. p. 1. Available at: https://www.esrl.noaa.gov/gmd/ccgg/trends/ (Accessed: 4 September 2018)
[2] Whipple, D.T., Finke, E.C., and Kenis, P.J. (2010). Microfluidic reactor for the electrochemical reduction of carbon dioxide: the effect of pH. Electrochemical and Solid-State Letters. 2010; 13(9): B109–B111. Available at: http://citeseerx.ist.psu.edu/viewdoc/download?doi=10.1.1.618.9980&rep=rep1&type=pdf
[3] Wang H., Leung DYC., Xuan J. Modeling of a microfluidic electrochemical cell for CO_2 utilization and fuel production. Applied Energy. 2013; Available at: DOI:10.1016/j.apenergy.2012.06.020
[4] Kjeang E., Djilali N., Sinton D. Microfluidic fuel cells: A review. Journal of Power Sources. 2009; Available at: DOI:DOI 10.1016/j.jpowsour.2008.10.011
[5] Bazylak A., Sinton D., Djilali N. Improved fuel utilization in microfluidic fuel cells: A computational study. Journal of Power Sources. 2005; Available at: DOI:10.1016/j.jpowsour.2004.11.029
[6] Chang MH., Chen F., Fang NS. Analysis of membraneless fuel cell using laminar flow in a Y-shaped microchannel. Journal of Power Sources. 2006; Available at: DOI:10.1016/j.jpowsour.2005.11.066
[7] Chen W., Chen F. Theoretical approaches to studying the single and simultaneous reactions in laminar flow-based membraneless fuel cells. Journal of Power Sources. 2006; Available at: DOI:10.1016/j.jpowsour.2006.07.049
[8] Chen F., Chang MH., Hsu CW. Analysis of membraneless microfuel cell using decomposition of hydrogen peroxide in a Y-shaped microchannel. Electrochimica Acta. 2007; Available at: DOI:10.1016/j.electacta.2007.05.072
[9] Li H., Oloman C. Development of a continuous reactor for the electro-reduction of carbon dioxide to formate - Part 2: Scale-up. Journal of Applied Electrochemistry. 2007; Available at: DOI:10.1007/s10800-007-9371-8
[10] Zhang Y., Mawardi A., Pitchumani R. Numerical studies on an air-breathing proton exchange membrane (PEM) fuel cell stack. Journal of Power Sources. Elsevier; 8 November 2007; 173(1): 264–276. Available at: DOI:10.1016/J.JPOWSOUR.2007.05.008 (Accessed: 3 August 2018)
[11] Ahmed DH., Park HB., Sung HJ. Optimum geometrical design for improved fuel utilization in membraneless micro fuel cell. Journal of Power Sources. 2008; Available at: DOI:10.1016/j.jpowsour.2008.06.045
[12] Wang XQ., Xu P., Mujumdar AS., Yap C. Flow and thermal characteristics of offset branching network. International Journal of Thermal Sciences. 2010; Available at: DOI:10.1016/j.ijthermalsci.2009.07.019
[13] Ebrahimi Khabbazi A., Richards AJ., Hoorfar M. Numerical study of the effect of the channel and electrode geometry on the performance of microfluidic fuel cells. Journal of Power Sources. 2010; Available at: DOI:10.1016/j.jpowsour.2010.06.094
[14] Shaegh SAM., Nguyen NT., Chan SH. An air-breathing microfluidic formic acid fuel cell with a porous planar anode: Experimental and numerical investigations. Journal of Micromechanics and Microengineering. 2010; Available at: DOI:10.1088/0960-1317/20/10/105008
[15] Delacourt C., Newman J. Mathematical Modeling of CO_2 Reduction to CO in Aqueous Electrolytes. Journal of The Electrochemical Society. 2010; Available at: DOI:10.1149/1.3502533
[16] Xuan J., Leung DYC., Leung MKH., Ni M., Wang H. A computational study of bifunctional oxygen electrode in air-breathing reversible microfluidic fuel cells. International Journal of Hydrogen Energy. 2011; Available at: DOI:10.1016/j.ijhydene.2011.04.151

[17] Wang H., Leung DYC., Xuan J. Modeling of an air cathode for microfluidic fuel cells: Transport and polarization behaviors. International Journal of Hydrogen Energy. 2011; Available at: DOI:10.1016/j.ijhydene.2011.08.033
[18] Krishnamurthy D., Johansson EO., Lee JW., Kjeang E. Computational modeling of microfluidic fuel cells with flow-through porous electrodes. Journal of Power Sources. 2011; Available at: DOI:10.1016/j.jpowsour.2011.08.024
[19] Xuan J. Theoretical Graetz–Damköhler modeling of an airbreathing microfluidic fuel cell. Journal of Power Sources. 2013; 110(231): 1–5.
[20] García-Cuevas RA. Toward geometrical design improvement of membraneless fuel cells: Numerical study. International Journal of Hydrogen Energy. 2013; 38(34): 14791–14800.
[21] Zhang, B., Ye, D. D., Sui, P. C., Djilali, N., & Zhu X. Computational modeling of air-breathing microfluidic fuel cells with flow-over and flow-through anodes. Power Sources. 2014; 259: 15–24.
[22] Yu Y., Zuo Y., Zuo C., Liu X., Liu Z. A hierarchical multiscale model for microfluidic fuel cells with porous electrodes. Electrochimica Acta. 2014; Available at: DOI:10.1016/j.electacta.2013.10.200
[23] Moein-Jahromi M., Movahed S., Kermani MJ. Numerical study of the cathode electrode in the Microfluidic Fuel Cell using agglomerate model. Journal of Power Sources. 2015; Available at: DOI:10.1016/j.jpowsour.2014.12.019
[24] Wu KN., Birgersson E., Kim B., Kenis PJA., Karimi IA. Modeling and Experimental Validation of Electrochemical Reduction of CO_2 to CO in a Microfluidic Cell. Journal of the Electrochemical Society. 2015; Available at: DOI:10.1149/2.1021414jes
[25] Jhong HR., Ma SC., Kenis PJA. Electrochemical conversion of CO_2 to useful chemicals: current status, remaining challenges, and future opportunities. Current Opinion in Chemical Engineering. 2013; Available at: DOI:10.1016/j.coche.2013.03.005
[26] Lu X., Leung DYC., Wang H., Leung MKH., Xuan J. Electrochemical Reduction of Carbon Dioxide to Formic Acid. ChemElectroChem. 2014; Available at: DOI:10.1002/celc.201300206
[27] Hori Y. Electrochemical CO_2 Reduction on Metal Electrodes. Modern Aspects of Electrochemistry. 2008. Available at: DOI:10.1007/978-0-387-49489-0_3
[28] Albo J., Alvarez-Guerra M., Castaño P., Irabien A. Towards the electrochemical conversion of carbon dioxide into methanol. Green Chemistry. 2015; Available at: DOI:10.1039/c4gc02453b
[29] Shamsipur M., Beigi AAM., Teymouri M., Pourmortazavi SM., Irandoust M. Physical and electrochemical properties of ionic liquids 1-ethyl-3-methylimidazolium tetrafluoroborate, 1-butyl-3-methylimidazolium trifluoromethanesulfonate and 1-butyl-1-methylpyrrolidinium bis(trifluoromethylsulfonyl)imide. Journal of Molecular Liquids. 2010; Available at: DOI:10.1016/j.molliq.2010.08.005
[30] Galiński, M., Lewandowski, A., & Stępniak I. Ionic liquids as electrolytes. Electrochimica acta. 2006; 51(26): 5567–5580.
[31] Shiflett, M. B., & Yokozeki A. Solubilities and diffusivities of carbon dioxide in ionic liquids:[bmim][PF6] and [bmim][BF4]. Industrial & Engineering Chemistry Research. 2005; 44(12): 4453–4464.
[32] Blanchard L a., Hancu D. Green processing using ionic liquids and CO_2. Nature. 1999; Available at: DOI:10.1038/19887
[33] Mihkel K ed. Ionic Liquids in Chemical Analysis: Analytical Chemistry. 1st edn. CRC Press; 2009. p. 448.